

Effect of Cr Content on the Electrochemical Behavior of Low-chromium X65 Steel in CO₂ Environment

Jianbo Sun^{}, Chong Sun, Yong Wang*

School of Mechanical and Electronic Engineering, China University of Petroleum, Qingdao 266580, PR China

*E-mail: sunjianbo@upc.edu.cn

Received: 13 July 2016 / Accepted: 23 August 2016 / Published: 6 September 2016

The electrochemical behavior of 1Cr, 3Cr and 5Cr steel in CO₂ environment was investigated in situ by means of electrochemical measurements. The characteristics of corrosion scale were characterized by surface analysis techniques. The results showed that 3Cr steel could reduce the corrosion rate by 51% compared with 1Cr steel, and the reduction in the corrosion rate slowed when the Cr content in X65 steel was higher than 3%. The Cr-rich corrosion scale on 1Cr, 3Cr and 5Cr steels possessed a prepassivation characteristic. When the Cr content was 3% or higher, an adequate amount of Cr compounds could form in the prepassivation film, which effectively inhibited the localized corrosion, while the pitting sources on 1Cr steel were developed to form the corrosion pits. The increase of Cr(OH)₃ content in the prepassivation film was conducive to improve the stability and compactness of the corrosion scale, and thus providing a favorable protection for the substrate, which was the reason why the CO₂ corrosion resistance of low Cr steel improved with the increase of Cr content.

Keywords: Low-chromium steel, CO₂ corrosion, Polarization curve, Electrochemical impedance spectroscopy, Corrosion scale

1. INTRODUCTION

CO₂ corrosion is one of the most serious problems in oil and gas fields due to the high general corrosion rate and severe localized corrosion [1-4]. One of the most common anti-corrosion measures is through alloying to improve the CO₂ corrosion resistance of steel [4-6]. Although corrosion resistant alloys (CRAs) such as stainless steels and high-nickel alloys have good CO₂ corrosion resistance, the high cost constrains the extensive application of CRAs in oil and gas fields. Therefore, carbon steel or low alloy steel is still the cost-effective material used for tubing and pipeline despite of the shortcoming of high corrosion rate [7-9]. In recent years, the novel Cr-containing (up to 5%) low alloy

steels possessing both good CO₂ corrosion resistance and low cost have been developed to fill the gap between CRAs and carbon steels [6, 9-14]. For example, 3% Cr steel can improve CO₂ corrosion resistance by a factor of 2.5-40 while maintain a cost penalty less than 1.5 times that of conventional grades of carbon steel [14, 15].

Previous research indicated that although the low Cr alloy steels with 0.5-2% Cr can reduce the CO₂ corrosion rate to some extent, it cannot avoid the localized corrosion effectively [6, 12, 14, 16, 17]. However, the low Cr alloy steels with 3-5% Cr not only reduce the CO₂ corrosion rate remarkably, but also avoid localized corrosion in CO₂ environment [6, 13, 18-20]. The improvement of CO₂ corrosion resistance of low Cr steel is mainly attributed to the formation of the amorphous Cr(OH)₃ in the corrosion scale that significantly changes the structure, compactness and stability of the corrosion scale [11-14, 18, 19]. Pigliacampo et al. [19] found that the addition of Cr could transform the corrosion scale from crystalline state to amorphous state, which resulted in the formation of denser corrosion scale and thus lowered the susceptibility of localized corrosion. Sun et al. [6] reported that corrosion scale of X65 steel containing 3-5% Cr was mainly composed of amorphous Cr(OH)₃ and FeCO₃, which could eliminate localized corrosion. However, most of the above research investigated the corrosion behavior of low Cr steel by means of weight loss method, which cannot provide sufficient information of electrochemical reaction in situ, especially that when the corrosion scale do not thoroughly cover the steel surface. Some research reported the electrochemical behavior of low Cr steel in CO₂ environment, but mainly focused on the 3Cr steel [21-23]. There are still not enough in situ electrochemical studies to determine the effect of Cr content on the electrochemical behavior of low Cr steel that is important for revealing the role of Cr and the optimal Cr content in low Cr steel.

The aim of this work is to investigate the effect of Cr content on the electrochemical behavior of low Cr steel in CO₂ environment. To achieve this objective, the electrochemical characteristics and the development of the corrosion scale on low Cr steel were determined in situ using potentiodynamic polarization curve and electrochemical impedance spectroscopy (EIS) technique. The morphology and composition of the corrosion scale were characterized by scanning electron microscope (SEM) and energy dispersive spectroscopy (EDS). Correspondingly, the relationship between the electrochemical behavior and the corrosion scale evolution was further discussed.

2. EXPERIMENTAL

2.1 Material and solution

Table 1. Chemical compositions of test steels (wt.%)

Steel	C	Si	Mn	Cr	Mo	Nb	V	Fe
1Cr-X65	0.07	0.20	0.55	0.95	0.15	0.03	0.03	Bal.
3Cr-X65	0.07	0.20	0.55	3.00	0.15	-	-	Bal.
5Cr-X65	0.07	0.20	0.55	5.00	0.15	-	-	Bal.

The test materials used in this study were 1Cr-X65, 3Cr-X65 and 5Cr-X65 steels and their chemical compositions are provided in Table 1. The specimens were machined into the size of 10 mm × 10 mm × 5 mm as working electrode (WE). Copper wire was welded to WE to ensure electrical contact for electrochemical measurements, and then WE was embedded in epoxy resin with exposed working area of 10 × 10 mm². Prior to the tests, the working surface of WE was abraded with silicon carbide paper of decreasing roughness (up to 800 grit), rinsed with deionized water and degreased with acetone.

The test solution, a 5 wt.% NaCl solution, was made up from analytical grade reagents and deionized water. The solution was purged with CO₂ (99.99%) for at least 4 h, and then WE was immersed into the solution while CO₂ gas purging was maintained at a low flow rate to ensure saturation throughout test.

2.2 Electrochemical measurements

A PARSTAT 2273 electrochemical test system was used for electrochemical measurements. A three-electrode electrochemical cell was used with a platinum plate as counter electrode and a saturated calomel electrode (SCE) as reference electrode. All the potentials in this study were referred to this reference electrode. Before potentiodynamic polarization curve and EIS tests, WE was immersed in the solution for 15-30 minutes to obtain a stable open circuit potential (OCP). EIS was measured at OCP with a sinusoidal potential excitation of 5 mV amplitude in the frequency range from 100 kHz to 5 mHz. Potentiodynamic polarization curves were carried out in a range of -250 mV~250 mV with respect to the corrosion potential, and with a scan rate of 0.5 mV/s. The impedance data were fitted with Zview software using an equivalent circuit.

All the tests were performed under static condition at 60 °C and atmospheric pressure (0.1 MPa) of CO₂. The tests were carried out for 6 h, 72 h, 168 h and 300 h respectively.

2.3 Characterization of the corrosion scale

The SEM morphologies and elemental compositions of the corrosion scale were investigated by Electron Probe Microanalyser (EPMA) (JEOL JXA-8230), equipped with an Energy Dispersive X-ray Spectroscopy (EDS) (Oxford INCA X-Act) with an acceleration voltage of 15 kV.

3. RESULTS AND DISCUSSION

3.1 Polarization curve analysis

Fig. 1 shows the potentiodynamic polarization curves of 1Cr, 3Cr and 5Cr steels exposed to CO₂-saturated solution at 60 °C. It can be seen that, in the tested range of Cr content, all the anodic polarization curves were flat with no obvious change in curve shape, indicating that the anodic dissolution reaction easily proceeded and the anodic polarization rate was low. Accordingly, the anodic

reaction mechanism of low Cr steel did not change with the increase of Cr content. However, the Tafel regions were clearly observed from the cathodic polarization curves, indicating that the resistance of the cathodic reaction was much larger than that of anodic reaction so that the electrode reaction rate was mainly controlled by the cathodic process.

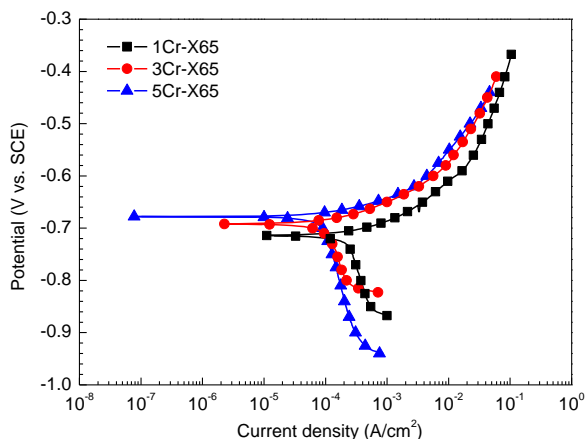


Figure 1. Polarization curves of X65 steels with different Cr contents in CO₂-saturated solution at 60 °C and 0.1 MPa.

Tafel's extrapolation method was employed to determine the corrosion current density. The fitted values of the electrochemical parameters such as corrosion potential (E_{corr}), corrosion current density (I_{corr}), anodic and cathodic Tafel slope (b_a and b_c) are listed in Table 2. Seen from Fig. 1 and Table 2, the polarization curves of low Cr steels shifted positively with the increase of Cr content, and correspondingly corrosion potential changed from -714 mV to -678 mV vs. SCE. Meanwhile, the cathodic and anodic polarization curves shifted to the left, and the corresponding Tafel slope obviously increased. It is indicated that the anodic process and cathodic process of low Cr steel were simultaneously suppressed with the increase of Cr content under test conditions. Compared with the corrosion current density (0.229 mA/cm^2) of 1Cr steel, the addition of 3% Cr could reduce the corrosion current density by 51 percent, i.e., a corrosion current density down to about 0.112 mA/cm^2 . The corrosion current density was further reduced to 0.089 mA/cm^2 when the Cr content in X65 steel increased up to 5%. The above results revealed that the reduction in the corrosion rate slowed when the Cr content in X65 steel was higher than 3%. Xu et al. [24] investigated the effect of Cr content ranged from 0 to 6.5% on the corrosion performance of low Cr steel at 80 °C and 0.8 MPa CO₂ by means of weight loss method also obtained the similar results. Therefore, 5Cr steel had highest CO₂ corrosion resistance under test condition, followed by 3Cr steel and 1Cr steel.

Table 2. Electrochemical parameters obtained from polarization curves of X65 steels with different Cr contents in CO₂-saturated solution at 60 °C and 0.1 MPa.

Steel	E_{corr} (mV vs.SCE)	I_{corr} (mA/cm ²)	b_a (mV/decade)	b_c (mV/decade)
1Cr-X65	-714	0.229	122	-358
3Cr-X65	-692	0.112	129	-385
5Cr-X65	-678	0.089	134	-466

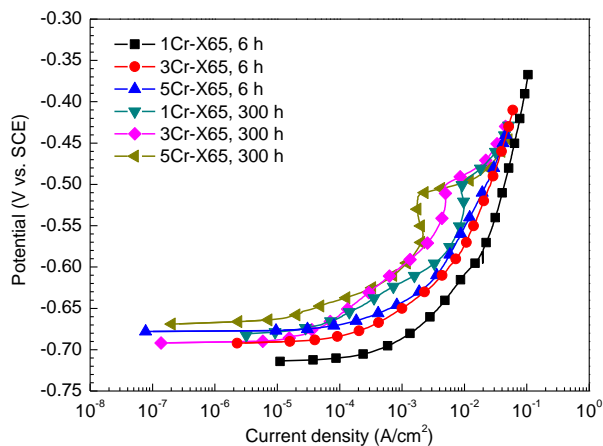


Figure 2. Anodic polarization curves of X65 steels with different Cr contents exposed to CO₂-saturated solution for 6 h and 300 h at 60 °C and 0.1 MPa.

Fig. 2 shows the anodic polarization curves of 1Cr, 3Cr and 5Cr steels exposed to CO₂-saturated solution for 6 h and 300 h at 60 °C. Compared with the flat curves at 6 h, a phenomenon of declined current density appeared in the anodic polarization curves at 300 h, which was similar to the characteristic of passivation. Xu et al. [24], Zhu et al. [21] and Guo et al. [22] also reported this phenomenon of low Cr steel, which was identified as “prepassivation” or “pseudopassivation”, and it was closely related to the formation of the Cr-rich corrosion products (Cr(OH)₃) on low Cr steel. And the prepassivation of the anodic polarization curves disappeared when the Cr content was lower than 3% [24]. However, the anodic polarization curve of 1Cr steel still presented the prepassivation under test condition. In addition, the anodic polarization curve of low Cr steel after corrosion for 300 h in CO₂ environment obviously shifted to the left compared with that in the early corrosion stage, which meant that the prepassivation film formed on low Cr steel provided a protection for the substrate and inhibited the anodic process. However, the anodic polarization curves also shifted to the left as the Cr content increased at 300 h. This indicated the protection performance of prepassivation film formed on low Cr steel changed with the Cr content.

3.2 EIS analysis and surface characterization of corrosion scale

Figs. 3-5 respectively show the SEM surface morphologies and cross-sectional backscattered electron images of the corrosion scales on 1Cr, 3Cr and 5Cr steels after corrosion for different corrosion time. It can be seen that, for the three steels, the corrosion scales presented the similar characteristics: the amorphous corrosion scales formed on the steel surface, and some corrosion products in the shape of spherical particles stacked on the surface of the amorphous corrosion scales. Related research suggested that the corrosion scale of low Cr steel is mainly composed of FeCO₃, Cr(OH)₃ and Cr₂O₃ [6, 9, 12-14]. Accordingly, with the corrosion scale on 5Cr steel, for example, the amorphous corrosion products and the granular corrosion products were respectively analyzed by EDS, the results showed that the amorphous corrosion products mainly contained 19.24% Cr, 16.06% Fe and 62.70% O elements while the granular corrosion products mainly 17.92% Fe and 52.93% O elements.

Therefore, it can be deduced that the corrosion scale of 5Cr steel mainly consisted of $\text{Cr}(\text{OH})_3$ and FeCO_3 .

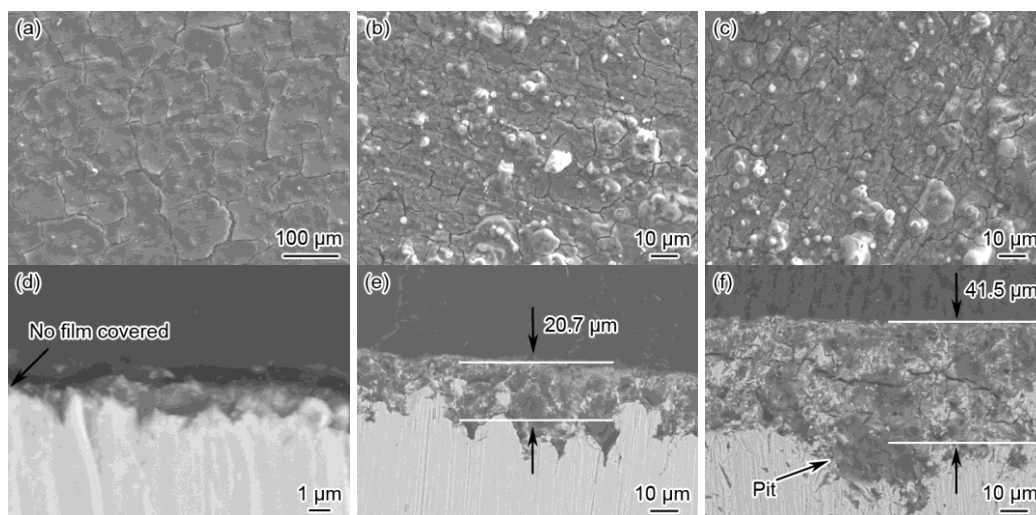


Figure 3. (a-c) SEM surface morphologies and (d-f) cross-sectional backscattered electron images of corrosion scale on 1Cr-X65 steel exposed to CO_2 -saturated solution for different corrosion time at 60 °C and 0.1 MPa: (a and d) 6 h; (b and e) 72 h and (c and f) 300 h.

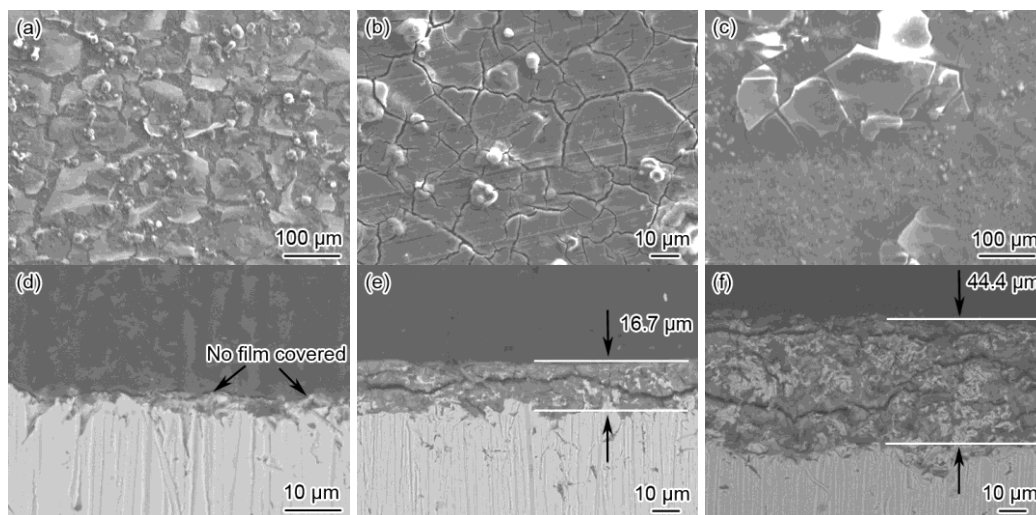
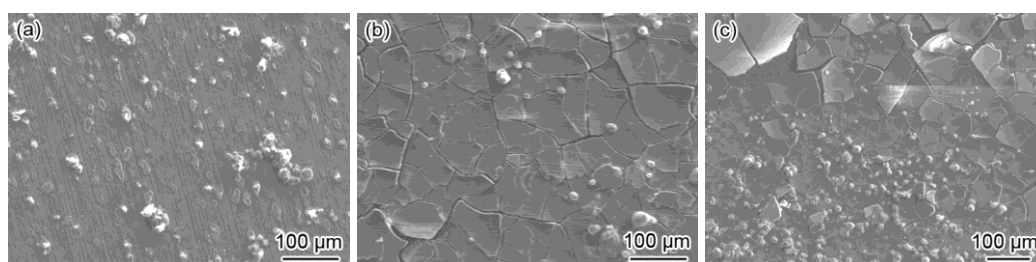


Figure 4. (a-c) SEM surface morphologies and (d-f) cross-sectional backscattered electron images of corrosion scale on 3Cr-X65 steel exposed to CO_2 -saturated solution for different corrosion time at 60 °C and 0.1 MPa: (a and d) 6 h; (b and e) 72 h and (c and f) 300 h.



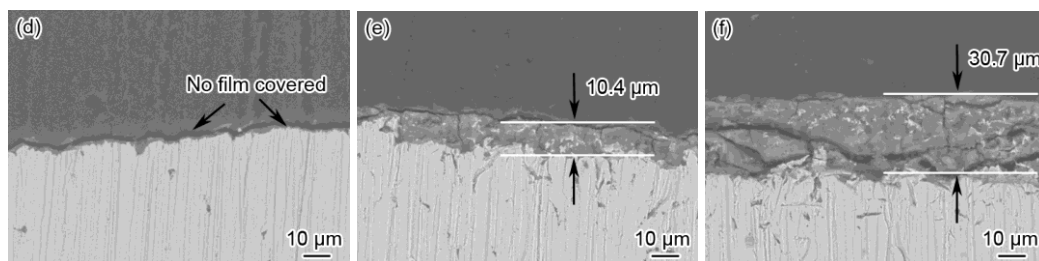
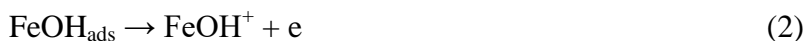


Figure 5. (a-c) SEM surface morphologies and (d-f) cross-sectional backscattered electron images of corrosion scale on 5Cr-X65 steel exposed to CO₂-saturated solution for different corrosion time at 60 °C and 0.1 MPa: (a and d) 6 h; (b and e) 72 h and (c and f) 300 h.

In the early corrosion stage, the steel surface exposed to CO₂-saturated solution suffered the rapid corrosion dissolution, and thus the produced Fe²⁺ and Cr³⁺ concentrations in the solution greatly increased, resulting in the increase of the supersaturation of Cr(OH)₃ and FeCO₃. Therefore, Cr(OH)₃ and FeCO₃ could deposit on the steel simultaneously over the first of 6 h (Figs. 3a, 4a and 5a). However, the corrosion scale was unable to cover the whole steel surface in the early corrosion stage. The cross-sectional morphologies of corrosion scale (Figs. 3d, 4d and 5d) showed that some regions without corrosion products covering were observed and the corrosion scale was very thin, only approximately 1 μm. Fig. 6 shows the EIS of 1Cr, 3Cr and 5Cr steels after corrosion for different corrosion time. It can be seen that there was a similar feature of Nyquist plots for the three test steels at 6 h, i.e., one depressed capacitive semicircle at high frequency, one inductive semicircle and one capacitive semicircle at low frequency. The capacitive semicircle at high frequency was attributed to the electrical double layer (EDL) capacitance and the charge transfer resistance [25-27]. The capacitive semicircle at low frequency was associated with the formation of corrosion products on the electrode surface [23, 25-27]. The inductive semicircle at low frequency was probably related to the adsorbed intermediate product FeOH_{ads} and CrOH_{ads} during the dissolution of electrode according to the following reactions [23, 28]:



The results of EIS indicated that the stable active regions and the coverage regions of corrosion products were present on the steel surface in the early corrosion stage [23, 29], which was accordance with the results of SEM morphology observation. In this case, it was impossible to form the stable and complete prepassivation film on the steel surface, therefore, the anodic polarization curves showed no prepassivation, as shown in Fig. 2. In addition, the initiation of the corrosion pits could be observed from the cross-sectional morphologies of 1Cr, 3Cr and 5Cr steels at 6 h (Figs. 3d, 4d and 5d). Related research indicated that the pitting sources existed at the interface between the corrosion scale and the steel substrate was in the induction period, and within the metastable state, which functioned as the

active points on the steel surface and could result in the occurrence of the inductive semicircle at low frequency. However, when the real pits appeared, the inductive semicircle at low frequency would disappear [30, 31]. Therefore, the electrode reaction was mainly controlled by active dissolution at 6 h.

As the corrosion proceeded, the coverage and thickness of corrosion scale on low Cr steel increased. At 72 h, the pitting source on 1Cr steel surface could be further developed (Fig. 3e), and the thickness of corrosion scale reached approximately 20.7 μm . At 300 h, the corrosion pit was observed obviously (Fig. 3f) and the thickness of corrosion scale increased up to 41.5 μm . By contrast, the pitting sources formed on 3Cr and 5Cr steels were not developed as the corrosion time prolonged (Figs. 4e and 5e). After corrosion for 300 h, the interface between the corrosion scale and the steel substrate was flat and presented general corrosion morphology (Figs. 4f and 5f). This indicated that the addition of 1% Cr into X65 steel did not avoid the localized corrosion. And the 3Cr and 5Cr steels not only greatly reduced the uniform corrosion rate but also inhibited the localized corrosion.

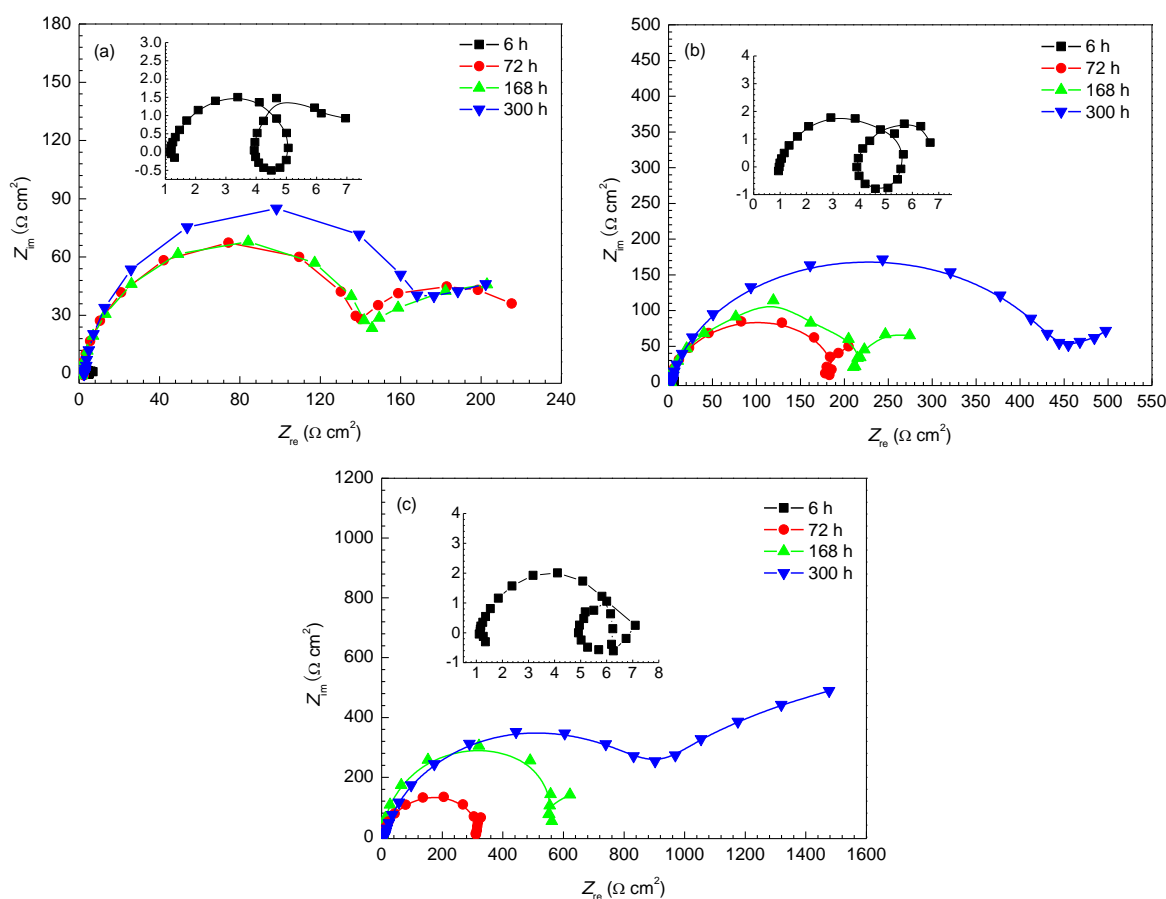


Figure 6. Nyquist plots of low Cr steels exposed to CO_2 -saturated solution for 6 h, 72 h, 168 h and 300 h at 60 °C and 0.1 MPa: (a) 1Cr-X65 steel; (b) 3Cr-X65 steel and (c) 5Cr-X65 steel.

See Fig. 6 for the EIS of the low Cr steel, the Nyquist plots gradually expanded outward with the increase of corrosion time. At 72 h and 168 h, all the Nyquist plots of the 1Cr, 3Cr and 5Cr steels showed one depressed capacitive semicircle at high frequency and one capacitive semicircle at low frequency, while the inductive semicircle at low frequency disappeared. In this case, the scale

completely covered the steel surface and there were no active regions in which bare steel was exposed to the solution. During this process, the electrode reaction began to be controlled by the diffusion process due to the complete corrosion scale with a certain thickness formed on the steel. However, all the Nyquist plots of the 1Cr, 3Cr and 5Cr steels showed one depressed capacitive semicircle at high frequency and the superposition of the capacitive semicircle and Warburg impedance at low frequency after corrosion for 300 h, indicating that the diffusion process mainly controlled the electrode reaction.

Table 3. The atomic ratio of Cr/Fe in the corrosion scale of low Cr steel after corrosion for 300 h at 60 °C and 0.1 MPa.

Steel	Cr/Fe ratio
1Cr-X65	0.220
3Cr-X65	0.442
5Cr-X65	0.597

EDS analysis of corrosion products in Figs. 3f, 4f and 5f were carried out. Accordingly, the atomic ratio of Cr/Fe in the corrosion scale was calculated, as listed in Table 3. It can be seen that the atomic ratio of Cr/Fe significantly increased, revealing that the Cr-rich degree in the corrosion scale improved with the increase of Cr content in the steel. The anodic polarization curves in Fig. 2 suggested that the Cr-rich corrosion scale formed on low Cr steel presented a prepassivation characteristic which had a role similar to that of the passive film of stainless steel [19, 22, 32]. Research indicated that the passive film of Fe-Cr alloy had a good protection for the substrate because of the high ratio of Cr/Fe, and the higher the ratio of Cr/Fe, the better the protection [33]. Guo et al. [22] investigated the corrosion behavior of 3Cr steel in CO₂ environment at 80 °C and 0.8 MPa and found that the Cr/Fe ratio of corrosion products on the pitting sources was higher than that of other parts of corrosion scale so that the pitting sources were inhibited. In this study, although the prepassivation film could form on 1Cr steel, its Cr/Fe ratio was far lower than that of 3Cr steel or 5Cr steel so that the pitting source formed on 1Cr steel in the early corrosion stage was further developed to form the corrosion pits. Hence, there must be an adequate amount of Cr compounds in the prepassivation film in order to effectively prevent the occurrence of localized corrosion. The anodic polarization curves of low Cr steel after corrosion for 300 h also showed that the potential range of prepassivation increased with the rising of Cr content, which revealed that the increase of Cr(OH)₃ content in the corrosion scale could improve the stability of corrosion scale, which provided a favorable protection for the substrate and thus reducing the corrosion rate of low Cr steel.

To quantify the EIS electrochemical parameters, the equivalent circuits were used for fitting the EIS data, as shown in Fig. 7. In the equivalent circuits, R_s is the solution resistance between working electrode and reference electrode; C_{dl} represents the EDL capacitance; L is the inductance induced by anodic dissolution, and R_L is the resistance of inductance component; R_t is the charge transfer resistance; C_f is the capacitance of corrosion products, and R_f is the resistance of corrosion products; Z_w is the Warburg impedance. The values of corresponding fitted electrochemical parameters are listed

in Table 4. Referring to the Figs. 3-5 and Table 4, when the intact corrosion scale formed on low Cr steel at the corrosion stage of 72 h-300 h, although the thickness of corrosion scale decreased with the increase of Cr content, the values of R_t and R_f noticeably increased with the rising of Cr content, indicating that the increase of $\text{Cr}(\text{OH})_3$ content in the corrosion scale was conducive to improve the compactness of corrosion scale, and the compact corrosion scale could restrain the corrosion by retarding the reactant diffusion and then slow down the corrosion rate of steel [34, 35].

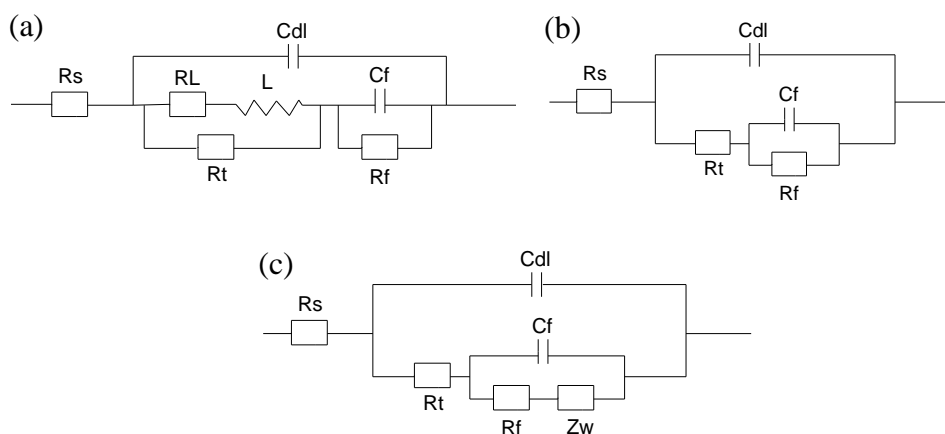


Figure 7. Equivalent circuits used for fitting EIS data of low Cr steel exposed to CO_2 -saturated solution for different corrosion time at 60 °C and 0.1 MPa: (a) 6 h; (b) 72 h and 168 h and (c) 300 h.

Table 4. Electrochemical parameters fitted from the measured EIS data of X65 steels with different Cr contents exposed to CO_2 -saturated solution for different corrosion time at 60 °C and 0.1 MPa.

Steel	Time (h)	R_s ($\Omega \text{ cm}^2$)	C_{dl} (F/cm^2)	R_t ($\Omega \text{ cm}^2$)	L (H cm^2)	R_L ($\Omega \text{ cm}^2$)	C_f (F/cm^2)	R_f ($\Omega \text{ cm}^2$)	Z_w ($\Omega \text{ cm}^2$)
1Cr-X65	6	1.27	1.70×10^{-4}	3.58	1.02	9.98	2.81	3.02	-
	72	1.52	9.26×10^{-4}	136.20	-	-	0.11	88.42	-
	168	1.42	1.35×10^{-3}	139.00	-	-	0.21	88.51	-
	300	2.65	3.05×10^{-3}	168.78	-	-	1.79×10^{-3}	149.80	3.01×10^{-2}
3Cr-X65	6	1.06	2.23×10^{-4}	4.34	1.14	8.08	2.74	3.14	-
	72	1.31	6.31×10^{-4}	183.41	-	-	5.25×10^{-4}	156.10	-
	168	2.47	5.06×10^{-4}	208.20	-	-	0.21	134.50	-
	300	3.66	1.76×10^{-4}	440.73	-	-	2.11×10^{-4}	206.50	3.93×10^{-2}
5Cr-X65	6	1.27	2.17×10^{-4}	4.69	1.66	15.09	1.67	1.82	-
	72	3.58	2.57×10^{-4}	286.55	-	-	3.96×10^{-4}	191.70	-
	168	12.87	7.67×10^{-4}	456.69	-	-	0.22	245.21	-
	300	7.46	0.18×10^{-4}	842.26	-	-	0.28×10^{-4}	271.8	9.32×10^{-2}

In contrast to the values of R_t and R_f , R_L and Z_w were relatively small and their changes were insignificant. Thus both R_t and R_f were the main resistances of corrosion process of the steel, a parameter named polarization resistance, R_p ($R_p = R_t + R_f$), was used to evaluate the corrosion rate of

the steel in CO₂ environment. There is an inversely proportional relationship between R_p and corrosion rate [8]. Fig. 8 shows that the relationship between R_p and the corrosion time. It can be seen that the R_p values of 1Cr, 3Cr and 5Cr steels were very small with little difference over the first of 6 h. Therefore, the electrode was in the stage of active dissolution, corresponding to a high corrosion rate. At the corrosion stage of 6 h-72 h, the R_p value rapidly increased with a high slope. And then the R_p value increased with a low slope and the change of corrosion rate approximately trended to be stable at the corrosion stage of 72 h-300 h. The decline in corrosion rate might be related to the accumulation of corrosion scale on the steel surface [14, 33, 36]. As exhibited in Figs. 3-5, the thickness of corrosion scale on low Cr steel surface increased as the corrosion time prolonged. The increase of corrosion scale thickness could lower the concentration gradient in it, which effectively reduced the flux of reactants and products through the corrosion scale, and the mass transfer process would gradually turned into the diffusion process [34], slowing down the corrosion of steel. Therefore, the Warburg impedance at low frequency appeared in the Nyquist plots of low Cr steels after corrosion for 300 h (Fig. 6).

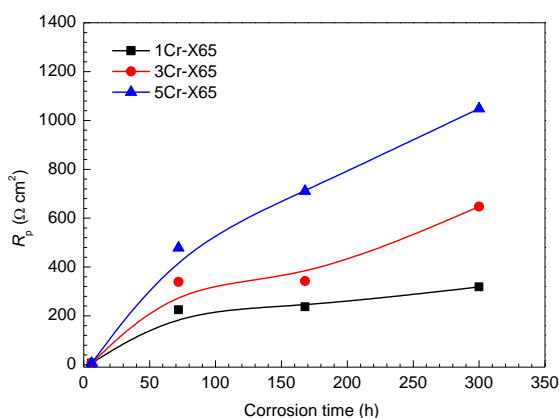


Figure 8. The polarization resistance of low Cr steel exposed to CO₂-saturated solution for different corrosion time at 60 °C and 0.1 MPa.

4. CONCLUSIONS

3Cr steel could reduce the corrosion rate by 51% compared with 1Cr steel, and the reduction in the corrosion rate slowed when the Cr content in X65 steel was higher than 3%.

The anodic polarization curves of 1Cr, 3Cr and 5Cr steels with the corrosion scale showed the phenomenon of declined current density which was similar to the characteristic of passivation. The Cr-rich corrosion scale on low Cr steel possessed a prepassivation characteristic.

The localized corrosion could be inhibited effectively when there was an adequate amount of Cr compounds in the prepassivation film of low Cr steel. The pitting source appeared on low Cr steel in the early corrosion stage. As the corrosion proceeded, the pitting sources on 1Cr steel were developed to form the corrosion pits, while that on 3Cr and 5Cr steels were inhibited.

Cr(OH)₃ content in the corrosion scale increased with the rising of Cr content, which could improve the stability and compactness of the corrosion scale, and thus providing a favorable protection for the substrate and reducing the corrosion rate of low Cr steel.

ACKNOWLEDGEMENTS

This work was supported by National Natural Science Foundation of China (No. 51471188) and Natural Science Foundation of Shandong Province (No. ZR2014EMM002).

References

1. M.B. Kermani, A. Morshed, *Corrosion*, 59 (2003) 659.
2. S. Nesic, *Corros. Sci.*, 49 (2007) 4308.
3. C. Sun, J.B. Sun, Y. Wang, S.J. Wang, J.X. Liu, *Acta Metall. Sin.*, 50 (2014) 811.
4. D.A. López, T. Pérez, S.N. Simison, *Mater. Des.*, 24 (2003) 561.
5. M.B. Kermani, J.C. Gonzales, C. Line, M. Dougan, R. Cochrane, Development of low carbon Cr-Mo steels with exceptional corrosion resistance for oilfield applications, *Corrosion/2001*, NACE, Houston, TX, 2001, Paper No. 01065.
6. J.B. Sun, W. Liu, W. Chang, Z.H. Zhang, Z.T. Zhang, T. Yu, M.X. Lu, *Acta Metall. Sin.*, 45 (2009) 84.
7. M. Kimura, Y. Miyata, K. Sakata, R. Mochiduki, Corrosion resistance of martensitic stainless steel OCTG in high temperature and high CO₂ environment, *Corrosion/2004*, NACE, Houston, TX, 2004, Paper No. 04118.
8. G.A. Zhang, Y. Zeng, X.P. Guo, F. Jiang, D.Y. Shi, Z.Y. Chen, *Corros. Sci.*, 65 (2012) 37.
9. Y. Xie, L.N. Xu, C.L. Gao, W. Chang, M.X. Lu, *Mater. Des.*, 36 (2012) 54.
10. H.B. Wu, L.F. Liu, L.D. Wang, Y.T. Liu, *J. Iron Steel Res. Int.*, 21 (2014) 76.
11. J.B. Sun, C. Sun, X.Q. Lin, X.K. Cheng, H.F. Liu, *Materials*, 9 (2016) 200.
12. Q.L. Wu, Z.H. Zhang, X.M. Dong, J.Q. Yang, *Corros. Sci.*, 75 (2013) 400.
13. C.F. Chang, M.X. Lu, D.B. Sun, Z.H. Zhang, W. Chang, *Corrosion*, 61 (2005) 594.
14. S.Q. Guo, L.N. Xu, L. Zhang, W. Chang, M.X. Lu, *Corros. Sci.*, 63 (2012) 246.
15. X.Q. Lin, W. Liu, F. Wu, C.C. Xu, J.J. Dou, M.X. Lu, Effect of O₂ on corrosion of 3Cr steel in high temperature and high pressure CO₂-O₂ environment, *Appl. Surf. Sci.*, 329 (2015) 104.
16. R. Nyborg, A. Dugstad, Mesa corrosion attack in carbon steel and 0.5% Chromium steel, *Corrosion/98*, NACE, Houston, TX, 1998, Paper No. 29.
17. C. Bosch, J.-P. Jansen, R.K. Poepperling, Influence of chromium contents of 0.5 to 1.0% on the corrosion behavior of low alloy steel for large-diameter pipes in CO₂ containing aqueous media, *Corrosion/2003*, NACE, Houston, TX, 2003, Paper No. 03118.
18. H. Takabe, M. Ueda, The formation behavior of corrosion protective films of low Cr bearing steels in CO₂ environments, *Corrosion/2001*, NACE, Houston, TX, 2001, Paper No. 01066.
19. L. Pigliacampo, J.C. Gonzales, G.L. Turconi, T. Perez, C. Morales, M.B. Kermani, Window of application and operational track record of low carbon 3Cr steel tubular, *Corrosion/2006*, NACE, Houston, TX, 2006, Paper No. 06133.
20. T. Muraki, K. Nose, H. Asahi, Development of 3% chromium linepipe steel, *Corrosion/2003*, NACE, Houston, TX, 2003, Paper No. 03117.
21. J.Y. Zhu, L.N. Xu, M.X. Lu, L. Zhang, W. Chang, L.H. Hu, *Corros. Sci.*, 93 (2015) 336.
22. S.Q. Guo, L.N. Xu, W. Chang, Y.R. Mi, M.X. Lu, *Acta Metall. Sin.*, 47 (2011) 1067.
23. J.Y. Zhu, L.N. Xu, M.X. Lu, *Corrosion*, 71 (2015) 854.
24. L.N. Xu, B. Wang, J.Y. Zhu, W. Li, Z.Y. Zheng, *Appl. Surf. Sci.*, 379 (2016) 39.
25. J.B. Sun, G.A. Zhang, W. Liu, M.X. Lu, *Corros. Sci.*, 57 (2012) 131.

26. G.A. Zhang, Y.F. Cheng, *Corros. Sci.*, 51 (2009) 87.
27. G.A. Zhang, Y.F. Cheng, *Corros. Sci.*, 51 (2009) 1589.
28. Z.F. Yin, W.Z. Zhao, Z.Q. Bai, Y.R. Feng, W.J. Zhou, *Electrochim. Acta*, 53 (2008) 3690.
29. C.F. Chen, M.X. Lu, G.X. Zhao, Z.Q. Bai, M.L. Yan, Y.Q. Yang, *Acta Metall. Sin.*, 38 (2002) 411.
30. C.N. Cao, J.Q. Zhang, *An Introduction to Electrochemical Impedance Spectroscopy*, Science Press, (2002) Beijing, China.
31. L.H. Hu, N. Du, M.F. Wang, Q. Zhao, *J. Chin. Soc. Corros. Prot.*, 27 (2007) 233.
32. X.H. Lu, Y.Q. Yang, G.X. Zhao, Z.H. Fan, Z.Q. Bai, M.X. Lu, *J. Mater. Sci. Eng.*, 22 (2004) 697.
33. D.J. Yang, Z.S. Shen, *Corrosion Science of Metal*, Metallurgy Industry Press, (1999) Beijing, China.
34. Y. Xiang, Z. Wang, Z. Li, W.D. Ni, *Corrosion* 69 (2013) 251.
35. Y.C. Zhang, X.L. Pang, S.P. Qu, X. Li, K.W. Gao, *Corros. Sci.*, 59 (2012) 186.
36. L. Wei, X.L. Pang, C. Liu, K.W. Gao, *Corros. Sci.*, 100 (2015) 404.

© 2016 The Authors. Published by ESG (www.electrochemsci.org). This article is an open access article distributed under the terms and conditions of the Creative Commons Attribution license (<http://creativecommons.org/licenses/by/4.0/>).